Energy and environmental analysis of ultrasound-assisted atmospheric freeze-drying of food.

Journal of Food Engineering [ISSN: 0260-8774], 283, 110031

DOI: 10.1016/j.jfoodeng.2020.110031

Energy and environmental analysis of ultrasound-assisted atmospheric freeze-drying of food

Merone, D.[a,b]; Colucci, D.[b]; Fissore, D.[b]; Sanjuan, N.[a]; Carcel, J. A.[a,*]

[a] ASPA Group, Department of Food Technology. Universitat Politècnica de València. Camino Vera s/n, 46022. València, Spain.

[b]Dipartimento di Scienza Applicata e Tecnologia, Politecnico di Torino, Corso Duca degli Abruzzi 24, 10129 Torino, Italy.

*Corresponding author:

Tel.: +34 963879365

jcarcel@tal.upv.es

Abstract

The atmospheric freeze-drying process can be significantly accelerated using power ultrasound. This paper aims to investigate the effects of this technology on the global energy consumption of the process and its environmental impact. Apple, carrot and eggplant were chosen as representative products because of their different internal structure and water content. A mathematical model of an industrial scale plant was developed to simulate *in silico* the atmospheric ultrasound-assisted freeze-drying process; model parameters were tuned according to the results obtained in a pilot-scale unit. Life Cycle Assessment (LCA) was used to gain an insight into the environmental impact of the process. The results showed that, when ultrasound is applied, the total energy consumption of the whole process can be reduced by up to 70%, while the LCA analysis proved there were reductions of between 58-82% depending on the product for every impact category. The moisture removal unit (dehumidifier) has been highlighted as the most critical stage. The internal structure of the product dramatically affects both the energy consumption of the process and, accordingly, the environmental impact.

Keywords: *atmospheric freeze-drying; ultrasonic; process modeling; Life Cycle Assessment*

1. Introduction

Drying is an energy intensive process, which employs 20-25% of the total energy consumed by the food industry (Kumar et al., 2014). For this reason, energy consumption, together with the quality of the dried products, are two critical parameters in the selection of a drying process (Sagar and Suresh Kumar, 2010). Alternative food drying processes, such as atmospheric freeze drying (AFD), have been proposed to improve the energy efficiency.

During the AFD process, water is removed from a frozen product by sublimation thanks to the difference between the vapor partial pressure of the ice and the drying chamber (Meryman, 1959). To guarantee and maintain this driving force, a stream of dry air is used as carrying agent to transport the moisture removed from the product and provide the energy required for ice sublimation (Claussen et al., 2007). This process offers several advantages with respect to the traditional batch vacuum freeze-drying: mainly, continuous processing, greater and more effective heat transfer to the product (as the heat transfer coefficient increases with pressure), and a reduction in the total energy consumption (Wolff and Gibert, 1990). Furthermore, it preserves the product quality because the process takes place at low temperatures (Stawczyk et al, 2008).

A typical AFD plant consists of a drying chamber and an air treatment unit (ATU). The latter usually includes (i) a cooling system, (ii) an air dehydration section to boost the global driving force for mass transfer, (iii) a fan for air velocity control, and (iv) a heating system for adjusting the air temperature at the required set point. The drying chamber is the place where the frozen product meets the stream of dried cold air and receives the energy required for ice sublimation, thus, reducing its moisture content. Different kinds of drying systems are used for industrial applications, among them the *tunnel freeze-dryer* and *fluidized bed* dryer.

In a tunnel freeze dryer, the previously frozen product is distributed on trays or on a belt conveyor, and the air stream flows in countercurrent. This is probably the most widely-used technology, despite the low turbulence achieved which decreases the mass and heat transfer rate at the solid-fluid interface. In a fluidized bed freeze-dryer, the air velocity required to fluidize the bed of the frozen product is high enough to provide good transfer coefficients. On the contrary, the occurrence of channeling and clogging effects, issues related to product recovery and to the small size and shape of the samples necessary for the purposes of easing fluidization, constitute the main challenges (Claussen et al., 2007).

The limiting step of the AFD process is its low drying rate; hence, several methods were proposed for its acceleration (Li et al., 2007). Rahman and Mujumdar suggested adding an absorbent material to the product to continuously dry the process air and take advantage of the heat released by water adsorption to speed up the sublimation rate (Rahman and Mujumdar, 2008). However, the separation of the desiccant from the dried product may be an issue and, the compatibility of the absorbent with the food product must be checked in every case.

Power ultrasound (US), i.e. acoustic waves with frequencies of between 20 and 100 kHz and a power of over 1 $Wcm^{-2,}$ appears to be particularly successful at increasing drying kinetics (Garcia-Perez et al., 2012; Santacatalina et al., 2015; Colucci et al., 2017), only slightly affecting product quality (Colucci et al., 2018), mainly because of the moderate thermal effect compared to other techniques, e.g. microwaves, infrared radiation or superheated steam.

The application of US to a porous matrix induces a series of rapid compressions and expansions. This provides an intense mechanical stress resulting in the formation of micro channels that speed up the water vapor removal through the natural product matrix. The mechanical energy supplied increases the diffusivity of water vapor inside the product matrix, leading to a rise in the effective mass transfer rate (Floros and Liang, 1994). US also improves heat and mass transfer at the solid fluid interface.

This effect is called *acoustic streaming* and consists of a partial conversion of the acoustic energy into a momentum gradient that reduces the boundary layer thickness controlling the mass and heat transfer (Lighthill, 1978).

The main limitation to the application of US to AFD and, in general, to any air-borne process, is the low density of air, which makes it a bad conductive medium, and its low acoustic impedance, which hinders the coupling with transducers (Garcia-Perez et al., 2015; Gottardo, 2016). However, a new generation of radiators with large surface area, developed by Gallego-Juarez et al. (1999), proved to be capable of overcoming these problems (Gallego-Juarez et al., 2007; Gallego-Juarez et al., 2010).

Both the product properties and the process variables can affect US efficiency. Along these lines, low porosity products absorb less acoustic energy, while the more power that is applied, the shorter the drying time becomes. Garcia-Perez et al. (2007) reported that the higher the temperature the lower the US efficiency. Those authors also observed that the turbulence induced by high air velocities could break down the acoustic field, reducing the amount of energy effectively provided to the product (Garcia-Perez et al. 2007). However, a rigorous investigation into the energy consumption and the consequent environmental impact of AFD processes and the effect of US is still lacking.

Life Cycle Assessment (LCA) has been widely used to estimate the environmental impact of a product or a process throughout its life cycle. In the last few years, the LCA of food products has increased considerably, although, to our knowledge, studies on dehydrated foods are scarce (Cieselski and Zbincinski, 2010; Prosapio et al., 2017; De Marco et al., 2015). The application of LCA to processes or products in the early stage of development is challenging. This is due, among other things, to the lack of reliable data (Hospido et al., 2010), since some studies use lab data, without taking into account scale considerations (Silva and Sanjuán, 2019).

To gain an insight into these issues, this paper aims to assess the energy consumption and environmental impact of the AFD of different foods with and without US application. Specifically,

three products with different porosities and textures were chosen as case studies, whose conventional and US-assisted drying kinetics were obtained from literature. Subsequently, the actual energy consumption of a laboratory dryer was measured under different drying conditions (US power, air velocity, etc) and for different products and empirical equations for the estimation of the energy consumption of the industrial dryer were developed for use in the framework of a mathematical model. This allowed the effect of the process variables involved to be calculated and the energy consumption of each of its components to be studied. Finally, the potential environmental impact of the process was calculated by applying LCA methodology in order to determine the most critical stages.

2. Materials and Methods

2.1. Raw materials and experimental set-up

Three different products were considered in this study, namely apple (*Malus domestica* cv. Granny Smith), carrot (*Daucus carota* L.) and eggplant (*Solanum melongena* L.). These products are characterized by very different internal structures, which explains their different porosity (0.423 for the eggplant, 0.233 for the apple and 0.031 for the carrot; Ozuna et al., 2014). The experimental drying kinetics (i.e. the effective moisture diffusivity in the dried product), with and without US, had previously been published (Garcia-Perez et al., 2012; Santacatalina et al., 2015; Colucci et al., 2017; Colucci et al., 2018): in particular, values of the moisture diffusivity were available for air velocity values of 1, 2 and 4 m s^{-1}, air temperature values of -10, 0, 10 and 20°C, and ultrasonic power values of 0, 10.3, 20.5 kW m^{-3} Therefore, the investigation carried out in the present paper will be focused mainly in the same range of drying operating parameters.

The experimental drying kinetics of these products were determined in a previously described lab-scale AFD dryer (Garcia-Perez et al., 2012), shown in Figure 1, which consists of a duralumin cylindrical chamber (10 cm diameter, 31 cm height and 1 cm wall thickness) into which food samples are placed. The chamber acts as an US radiator, being directly connected to a piezoelectric transducer, with 21.9 kHz average frequency, 369 Ω impedance and a maximum power capacity of 90 W. The electrical input is produced by a generator (APG-AC01, Pusonics, Spain) and the working frequency is continuously adapted and amplified (RMX4050HD, QSC, USA) to minimize the phase. The required air flow rate is obtained through a fan, while the air leaving the drying chamber is recycled. The drying air temperature is controlled by the combined action of a heat exchanger (finned surface cross flow heat exchanger, Frimetal, Spain. Total area: 13 m^2, fin space: 9 mm), using a glycol–water solution (45% v/v) at -19 °C, and an electric resistance. The air stream is then forced to pass through a bed of desiccant material, which is periodically changed and regenerated (7 hours at 250 °C) and permits the relative humidity of the drying air to be kept below 10 % during the whole drying process.

The electric power consumption of the elements of the system (fan, ultrasonic generator and heating resistance) with the drying conditions presented above was experimentally measured by means of a power quality analyzer (Fluke 435, Fluke Corporation, Holland).

2.2. Mathematical modeling at lab scale

The power consumption of the US system was estimated as a function of the power applied, the air temperature and the air velocity. First, the energy consumption at 0 kW m^{-3} for different air velocity and temperature values was measured; then, the same measurements were repeated for each combination of the operating conditions with different values of ultrasonic power applied, namely 10.3 and 20.5 kW m^{-3}. The energy consumption when applying US was obtained as the difference between

the measurements obtained with and without US. In this way, the effect of all three process variables was assessed.

The energy consumption of the different sections of the dryer was modeled. An average temperature drop of 1°C was considered in the drying chamber due to the energy exchange with the external environment, regardless of the operating conditions. As for the cooling air system used, the temperature at the heat exchanger's exit was calculated according to a heat balance:

$$U_{global} A \Delta T_{m,l} = m_{air} C_{p,\mathrm{air}} \Delta T_{air} \quad (1)$$

where A is the actual exchange area of the equipment obtained from the catalogue of manufacturer (Frimetal, Spain), i.e. 13 m^2, U_{global} is the global heat exchange coefficient for a mixed flow crossflow heat exchanger, which was assumed to be equal to 50 $W \cdot m^{-2} \cdot K^{-1}$ (Kern, 1950). m_{air} and $C_{p,air}$ are the mass and specific heat of the air flow respectively, while ΔT_{air} is the net temperature in the air flow between the inlet and the outlet of the exchanger and $\Delta T_{m,l}$ is the logarithmic mean temperature difference, that is, the driving force to heat exchange.

The energy consumption as a result of the passage of drying air through the desiccant material was also taken into consideration. Since the dehumidification process is exothermic, the air temperature increase at the exit to this section was calculated as the sum of the heat released by means of the absorption of the water molecules on the desiccant surface and the heating due to the humidity decrease in the air ΔU:

$$\Delta T_{dehumification} = \frac{G \Delta H_s}{m_{air} C_{p,air}} + \frac{m_{air} \Delta H_v \Delta U}{m_{air} C_{p,air}} \quad (2)$$

The heat of absorption was assumed to be equal to the sublimation enthalpy, ΔH_s, whereas ΔH_v is the heat of vaporization (Aermec, 2018). G is the sublimation flux, i.e. the water vapor removal rate.

The dry air then goes through a fan, which must compensate for the pressure drop in this device (Figure 1) in order to provide the desired air velocity. Furthermore, pressure drops inside the cooling heat-exchanger, the dehumidifier and the drying chamber were modelled as well. Given the random disposition of the product inside the drying chamber, the exact description of the total pressure drop would have required a very complex 3D fluid dynamic study. In this study, it was assumed the samples in the drying chamber behave as a fixed bed at high void degree, where the Ergun equation applies (Ergun, 1952). Thus, given the total volume of the chamber, $V_{chamber}$, and the volume of the product, $V_{product}$, the void fraction, ε, was calculated as:

$$\varepsilon = 1 - \frac{V_{product}}{V_{chamber}} \tag{3}$$

The total pressure drop reads as follows:

$$\Delta P_{TOT} = \Delta P_{line} + \Delta P_{Dehumidifier} + \Delta P_{chamber} + \Delta P_{heatexchanger} \tag{4}$$

The air stream was considered incompressible, due to the low pressure drop. Under this hypothesis, the power supplied by the fan is given by:

$$P_{fan} = \frac{V_{air} \Delta P_{TOT}}{\eta_{fan}} \tag{5}$$

where V_{air} is the volumetric air flow, and η_{fan} is the compressor efficiency.

Given a certain efficiency of the system, η_{res}, the power required by the heating resistance used to control the air temperature reads:

$$P_{resistance} = \frac{m_{air} C_{p,\mathrm{air}} \Delta T_{air}}{\eta_{res}} \tag{6}$$

The efficiencies of the fan and the resistance are unknown *a priori* and were fitted from the experimental results.

2.3. Industrial-scale dryer simulation

To assess the effect of the operating conditions on the energy consumption of a real freeze-drying process for commercial purposes, industrial-scale equipment was designed and simulated to process 100 kg of fresh product per batch. As in the previously described lab-scale unit, the industrial plant includes a drying chamber and an ATU unit. Thus, the model developed for the lab-scale equipment was adapted to simulate the industrial equipment together with the correlation obtained for the energy consumption of the US generation system.

A scheme of the industrial-scale dryer is shown in Figure 2. The drying chamber has drilled shelves of 2 x 1 m^2, on which the frozen product is placed, and a shelf-to-shelf distance of 0.1 m. The configuration of the drying chamber was similar to the one reported by Colucci et al. (2017).

As ice sublimation is endothermic, the dry cold air flows continuously, supplying energy to the product and removing its moisture. The US radiators have been designed to provide an effect as uniform as possible. Radiating plates were thus introduced between each pair of trays. The outlet air is then filtered and cooled in such a way that the moisture is partially removed. The heat exchanger used to cool the air stream uses a glycol-water-solution (60% v/v), regenerated in a refrigerating circuit using R134A as technical fluid. This system also encompasses a desiccant wheel, that is, a drum full of desiccant material slowly rotating on its axis. Usually, three quarters of its surface are devoted to moisture removal from the air stream, while the rest is continuously regenerated using superheated steam or, a portion of the initial air stream. An electrical heating system is used to increase the temperature of this stream when needed.

The air temperature increases when passing through the desiccant. For this reason, the air temperature at the exit of the desiccant wheel was calculated by applying the approach used for the silica packed bed of the lab-scale equipment (Eq. 2). The mild temperature increase was compensated

for a cooling system placed before the entrance of the drying chamber which brought the process air to the required temperature. The technical fluid of this last heat exchanger is water at -15 °C. A feedback controller guarantees the air flow rate and temperature.

Table 1 shows the energy required by the desiccant system (Aermec, 2018; Munters, 2018), the efficiencies of the filtering systems (Tecno-Ventil, 2018), the desiccant wheel (Puaide, 2018) and cooling systems (Tefrile, 2018), which were taken from the manufacturer catalogues.

All the heat exchangers used in the process are of the same kind and dimensions for the sake of simplicity in the warehouse management and were designed using the ε-NTU method (Incropera and DeWitt, 1990).

Air-handling systems are used to drive the stream of air through the drying chamber and the regeneration system. The power used by the fan for air velocity control was calculated as in Eq. (5), but the pressure drops inside the two filters were added to ΔP_{tot} in Eq. (4) according to Eqs. (7) and (8).

$$\Delta P_{G4} = \frac{7.543}{2} v_{air}^{1.9865} \tag{7}$$

$$\Delta P_{F7} = \frac{18.783}{2} v_{air}^{1.8431} \tag{8}$$

where v_{air} is the air velocity and Eq. (7) and Eq.(8) were obtained from the manufacturer catalogue (Camfil, 2018).

2.4 Life Cycle Assessment

A comparison of the environmental impact of the simulated AFD in an industrial-scale process for the studied products, with and without ultrasound assistance (ultrasonic power 20.5 kW m^{-3}), was carried out through LCA according to the ISO standards (2006a; 2006b).

The functional unit to which all the process inputs and outputs were related was 1 kg of fresh product, namely eggplant, apple or carrot, to be dehydrated. Gate-to-gate system boundaries were set

(Figure 3), since both previous and subsequent life cycle stages (e.g. raw material production, packaging, transportation) are the same regardless of the process considered, namely AFD or US-assisted AFD. The manufacturing of capital goods was not included, since the equipment is the same in both processes, except for the US generator. Considering that the system is supposed to work 24 hours per day and the life of the US generator is around 10 years, when the environmental load of its manufacturing is allocated, the generator has a negligible impact.

As for the life cycle inventory, process data on power consumption were obtained from the mathematical simulation of the industrial plant, while the energy consumption of the freezing step was estimated following Sanjuán et al. (2014). Background data (production of electricity, ethylene glycol and refrigerants R152A and R134A) were obtained from the Ecoinvent 3.5 database. In the initial freezing step and the cold battery, a 5% annual leakage for both ethylene glycol and refrigerant R134A was considered, according to Hoang et al (2016).

ReCiPe 2016 v1.1 (Huijbregts et al., 2016) was used under a hierarchical approach to calculate the following impact categories (category indicators in brackets): climate change (kg CO_2 eq.), fine particulate matter formation (kg PM2.5 eq.), fossil depletion (kg oil eq.), freshwater eutrophication (kg P eq.), freshwater ecotoxicity (kg 1,4 DB eq.), human toxicity, cancer and non-cancer, (kg 1,4-DB eq.), ionizing radiation (Bq C-60 eq. to air), marine ecotoxicity, (kg 1,4-DB eq.), marine eutrophication (kg N eq.), metal depletion (kg Cu eq.), photochemical oxidant formation, ecosystems and human health (kg NMVOC eq.),water depletion (m^3), stratospheric ozone depletion (kg CFC-11 eq.), terrestrial acidification (kg SO2 eq.), and terrestrial ecotoxicity (kg 1,4-DB eq.) GaBi 8 software (Thinkstep, Leinfelden-Echterdingen, Germany) was used for the analysis.

To examine the influence of some parameters, several scenarios were tested for the case study of eggplant processed with US-assisted AFD. As shown in Table 2, these scenarios concern different

electricity country mixes and solutions to reduce environmental impacts, namely R152A as an alternative refrigerant with lower global warming potential, and the self-production of electricity by installing photovoltaic panels on the roof (process from Ecoinvent v.3). European grid mixes are very diverse in Europe and can thus have different environmental impacts. Specifically, mixes from Spain, Denmark and Norway were considered (processes from Ecoinvent v.3.5 database).

3. Results

3.1. Energy consumption analysis – Lab scale

The values of the actual energy consumption per hour of the different units of the lab-scale dryer were experimentally determined in different process conditions and for all three materials studied. Thus, for example, the values of energy consumption obtained when the air velocity was 1 m s^{-1} ranged from 0.142 kWh h^{-1} at 0 W to 0.526 kWh h^{-1} at 20.5 kW m^{-3} of ultrasonic power. These experimental values were compared to those calculated through the proposed equations (Eqs. 1 to 6). In this way, the adequacy of these equations was proven, and the missing parameters that best fit the experimental results were estimated. The fan and heating resistance efficiencies, η_{fan} and η_{res} were calculated, obtaining values of 0.298 and 0.95, respectively. By using these parameters, the error between the experimentally measured energy consumption and the calculated one ranged from 0.25% to 6.25%, depending on the operating conditions considered. These efficiencies were constant for all the different products considered, the only substantial difference in their energy consumption was the time required for their total drying, which depends on the product stiffness and porosity.

Next, the influence of the process variables on the energy consumption of the ultrasonic generation system was studied. In this case, taking into account the specific features of the experimental apparatus used in this study, the range of values of the ultrasonic power investigated

experimentally was slightly larger than that considered in previous studies. The experimental results showed that the effect of the air velocity on the energy consumed was negligible, regardless of the product. The system can compensate for small deviations induced in the impedance of the medium by adjusting the generation frequencies. On the other hand, the higher the air temperature and the more ultrasonic power applied, the greater the energy consumed by the system (Figure 4). An equation was proposed to relate these parameters:

$$P_{US} = 10^{-3} I_{US} + 2 \cdot 10^{-5} T_{air}^{1.6} \quad (9)$$

where P_{US} is the power required by the US generating system (kW m^{-3}), I_{US} is the ultrasonic power (kW m^{-3}) and T_{air} is the air temperature. While the effect of the applied ultrasonic power (in the range of US intensities considered) on the consumption was linear as expected, the effect of air temperature was not. Eq. (9) was used to calculate the total energy consumed in the simulation of the industrial scale unit.

Figure 5 compares the total energy consumption per kilogram of water removed, measured in the lab-scale equipment, for different values of ultrasonic power and air velocity. Although the data reported in Figure 5 refer to eggplant drying, similar trends were obtained for the other two test cases, i.e. carrot and apple. The higher the air flow rate, the greater the energy consumption, despite their minimum effective contribution to the acceleration of the drying process. In fact, air velocity only affects the external resistance to mass transfer and, since in AFD it is the internal mass transfer which controls the drying rate, the mild reduction in the drying time that the increase in air velocity produces does not compensate for the higher energy requirement of the fan.

US application dramatically reduces the drying time. Thus, in the case of drying eggplant at an air velocity of 4 m s^{-1}, the energy required when an ultrasonic power of 10.3 kW m^{-3} was applied was

50% lower than that required when no ultrasound was applied. However, when moving to the maximum ultrasonic power tested (20.5 kW m^{-3}), only a slight further reduction was obtained.

Once the model of the lab-scale dryer was validated, the energy consumption calculated for each one of the different components of this equipment was studied and compared at the different levels of ultrasonic power applied. The relative amount of energy consumed per hour by the US generator, the compressor and electrical heater are compared in Figure 6. As expected, the increase in ultrasonic power produced a significant growth in its relative contribution to the total energy consumption of the dryer. This contribution increased by up to 60% when the maximum ultrasonic power (20.5 kW m^{-3}) was applied. US application increased the sublimation rate, and then the moisture content in the air. However, this did not lead to an effective increase in the relative contributions to the energy consumption of the fan and the heating resistance. The proportion between the two is mostly constant, with the consumption of the fan roughly 12 times that of the heating resistance.

3.2. Energy consumption analysis – Industrial simulated plant

The efficiency of the fan and the heating resistance estimated from the experimental measurements and the lab-scale modelling were used together with Eq. (9) in the model of the industrial atmospheric freeze dryer presented in section 2.3: results are shown in Figure 7.

The different drying rates of the products considered in this study, probably linked with the different internal structure, were observed to lead to relevant variations in energy consumption. The shorter the drying process the lower energy consumption. Thus, the energy consumed during the conventional AFD (without ultrasound, 0 kW m^{-3}) of eggplant, the product with highest drying rate tested, was 12% of the consumed in the drying of carrot, the product with the lowest drying rate tested (Figure 7). An energy reduction of about 70% was obtained in those drying experiments with an ultrasonic power of 10.3 kW m^{-3}, regardless of the product processed. This means that, although the use of US increases the energy consumption per hour (kWh h^{-1}), the shorter processing time lowers

the energy consumption of the whole process (kWh). It can thus be stated that the application of ultrasound increases the energy efficiency of the AFD process. This efficiency is indeed dependent on the internal structure of the product, that is, its porosity, which affects the actual moisture diffusivity and, therefore, the process time and energy consumption. An optimal value of ultrasonic power corresponding to the minimum energy required was observed (Figure 7). This minimum was identified at 31.6 kW m^{-3} for eggplant, 45.0 kW m^{-3} for apple and 49.3 kW m^{-3} for carrot, respectively, being the trend of these values inversely proportional to the porosity of the products. When the ultrasonic power is above this minimum, the increase in the amount of energy required for its generation is only partially compensated for by the drying time reduction. Drying one kilogram of carrots under these optimal conditions requires almost ten times the energy needed for the same quantity of eggplants, i.e. 599.6 kWh and 60 kWh respectively. AFD is not a feasible option for drying carrots or, in general, for any of those products whose inner matrix appears particularly compact.

Figure 8 shows the relative contribution of each main component to the total energy consumption of the industrial dryer. When no ultrasonic power is applied, the moisture removal unit exhibits the highest energy consumption (67.5% of the total consumption). The cooling and heating systems together contribute approximately one third of the total consumption and the contribution of the fan only accounts for 3.8% of the energy demand. When ultrasound is applied, the weight of the energy consumption of each part of the dryer relative to the total energy follows a similar trend to that experimentally determined for the lab equipment. The relative energy demand of the US generation system almost reaches 44% of the total energy, whereas the relative contribution of the remaining components of the dryer to the energy demand is significantly reduced to around half the energy demand without US. In any case, as observed in the lab-scale dryer, the drying time reduction compensates for the increase in energy consumption per hour that US application involves.

3.3. Environmental assessment

In this section, the results of the LCA for the AFD with and without US on an industrial scale are presented for the analyzed products. As pointed out in Section 2.4, the energy results from the simulation were used as inventory data. Hence, the LCA results are related to the energy consumption of the process, showing that, as expected, the use of US could reduce all the impact indicators with respect to the conventional AFD for each one of the three products studied (Table 3). Reductions in the impact categories were between 58-82%, depending on the product and the impact categories.

The contribution of the different process stages and elements of the drying equipment to the impact results are explained below for the case of eggplant, although the trend is similar for the remaining studied products. For the contribution analysis, it has been considered that the system comprises a blast air freezer, where the samples are frozen before being processed by AFD, and the industrial AFD dryer depicted in Section 2.3. The industrial AFD dryer consists of the following elements: a drying chamber which includes the fan and the US generator (when needed); a cooling unit where the temperature of the exhaust air from the dryer is reduced, a moisture removal unit where the water from the air is removed and a heater.

In the conventional AFD of eggplant, as can be observed in Figure 9, the contribution of the dryer elements to the impact categories can be ranked according to the energy consumption previously shown (Figure 8). Therefore, the dehumidifier, which exhibits the highest energy consumption, is the one contributing the most to all the impact categories: for instance, it accounts for 36% of the total photochemical ozone formation-ecosystems, 46% of climate change and 50% of particulate matter formation, marine eutrophication and terrestrial acidification. The heater is responsible for 30 to 39% of the impact categories, also due to the electricity consumption. The contribution of the cooling unit to the impacts varies depending on which one is considered: 33% of the total photochemical ozone formation-ecosystems, 14% of climate change and metal depletion, 12% of stratospheric ozone

depletion, etc. As to the contribution of the cooling unit to climate change, it is produced not only by the emissions associated with the electricity consumption, but also by the refrigerant leakage, since R134A is a fluorinated gas with a high global warming potential. The leakage of ethylene glycol in the same process unit is the reason for its significant contribution to the formation of photochemical ozone, whereas the production of this refrigerant to compensate for the leakage explains the impact of metal depletion. The drying chamber, which only includes the power consumption of the fan, and the freezer make the lowest contributions to all the impact categories, between 2-3% and 1% or less, respectively. When applying US to the AFD of eggplants (Figure 10), it can be observed that the dehumidifier is the one contributing the most to all the impact categories (40 to 45% of the corresponding impact), followed by the drying chamber (26 to 29% of the corresponding impact), the heater (17 to 19% of the total corresponding impact) and the cooling unit (7 to 17% of the total impact); once again the freezer is the process unit making the lowest contribution to all the impact categories (1% or less). When comparing these results with the ones without US application, the greater contribution of the drying chamber to all the impact categories is due to the fact that, in this case, it includes the power consumption from the US transducer.

LCA data on the agricultural stage of eggplant highlight the low contribution of this stage for a potential "cradle to grave" study. In particular, the contribution of the agricultural stage to climate change is 0.25 and 2.0 kg CO_2 eq, for Spanish and Dutch eggplant, respectively (Scholz et al., 2015). Hence, considering the results of the industrial processing from Table 3, the farming stage accounts for 0.2% and 1.7% of the total CC impact of AFD, for Dutch and Spanish raw material, respectively; however, when considering US- AFD, it accounts for 0.7% and 5.3% of the total CC for Dutch and Spanish raw material.

As pointed out in the introduction, LCA studies into the drying or freeze drying of food are scarce and, to our knowledge, studies into AFD are not available. In the following lines, however, the climate change impact values from studies into different food dehydration techniques are commented on. For instance, in an LCA of apple dehydration (De Marco et al.; 2015), the impact of the processing stage was 0.25 kg CO_2 eq./kg fresh apple and 0.075 kg CO_2 eq./kg fresh apple, for drum drying and multi-stage drying respectively. Prosapio et al (2017) analyzed the impact of freeze-dried strawberries, this being 0.22 kg CO_2 eq./kg fresh strawberry, the impact decreasing to 0.116 kg CO_2 eq./kg fresh strawberry when an osmotic pretreatment was applied. It must be taken into account that the moisture content of the freeze-dried strawberries was 7.4 % (w/w) (Prosapio et al., 2017), whereas in the present study the products are supposed to reach 0% (w/w) moisture content, which could explain the greater contribution of the present study to the climate change impact. In any case, measures to decrease the energy consumption of US-assisted AFD should be implemented to make it more advantageous from both the environmental and economic points of view.

Scenarios for eggplant processed through US-assisted AFD with grid mixes from different countries were assessed to evaluate how the share of energy production affects the functional unit (Table 3). The performances of different countries may be observed to vary greatly. The Norwegian electricity mix is the one that decreases all the impact categories the most, by around 90%. Both the Spanish and German electricity grids are beneficial for some impact categories, e.g. the Spanish mix decreases the ozone depletion in the stratosphere by 64%. However, they are detrimental for other impacts, for instance, both the Spanish and German mixes increase the ionizing radiation more than 2000% with respect to the Italian grid mix. As to the use of R152a as a refrigerant to decrease direct emissions from leakage, a slight decrease in the impact values was observed, mainly in the cases of climate change and photochemical ozone formation. On the other hand, the installation of photovoltaic panels would considerably decrease some impact categories, such as climate change (84% reduction), fossil

depletion (85%) or stratospheric ozone depletion (88%). However, a great increase in toxicity-related impacts, ionizing radiation and metal depletion was observed.

4. Conclusions

In this study, the effects of the application of US to the AFD process were studied in terms of a trade-off between the well-known effects of process acceleration, that is, increased productivity, and their energy consumption and environmental impacts.

From the energy consumption point of view, although the application of US in an AFD process accounts for over 50% of the relative energy consumption, it significantly shortens the drying time; thus, compared to the conventional process, up to 70% of the total energy required by the process (depending on the product) can be saved. In fact, an optimum ultrasonic power can be identified for each product which accelerates the drying process while minimizing the energy consumption. Considering the values of kWh per kg of product processed, the process appears particularly attractive for highly porous products.

The LCA results show that, with respect to conventional AFD, a 58-82% reduction in every impact category studied was obtained when applying US, depending on the product and the impact category. However, in comparison with other dehydration techniques found in the literature, the impact of US-assisted AFD is significant; therefore, although product quality is high, measures to reduce energy consumption should be implemented to make it more advantageous from both the environmental and economic points of view.

It must be noted that the methodology followed in this study, being more physically grounded than a simple comparison of an estimated parameter, could be used for the purposes of effectively comparing different drying processes.

Acknowledgment

The authors acknowledge the financial support of INIA-ERDF throughout project RTA2015-00060-C04-02.

References

Aermec (2019). L'aria umida e l'uso del diagramma psicrometrico. http://web.taed.unifi.it/fisica_tecnica/Cellai/uso_del_diagramma_psicrometrico.pdf (Accessed: 18/06/2019).

Camfil (2019). The energy and filter fact handbook. https://www.camfil.com/damdocuments/38999/energy-and-filter-fact-handbook.pdf (Accessed: 18/06/2019).

Ciesielski, K., & Zbicinski, I. (2010). Evaluation of environmental impact of the spray-drying process. *Drying Technology*, 28(9), 1091-1096.

Claussen, I. C., Andresen, T., Eikevik, T. M., & Strommen, I. (2007a). Atmospheric freeze drying-Modelling and simulation of a tunnel dryer. *Drying Technology*, 25, 1959-1965.

Claussen, I.C., Ustad, T.S., Strommen, I., & Walde, P.M. (2007b). Atmospheric freeze drying- A review. *Drying Technology*, 25, 957–967.

Colucci, D., Fissore, D., Mulet, A., & Carcel, J. A. (2017). On the investigation into the kinetics of the ultrasound assisted atmospheric freeze drying of eggplant. *Drying Technology*, 35, 1818-1831.

Colucci, D., Fissore, D., Rossello, C., & Carcel, J.A. (2018). On the effect of ultrasound-assisted atmospheric freeze-drying on the antioxidant properties of eggplant. *Food Research International*, 106, 580-588.

De Marco, I., Miranda, S., Riemma, S., & Iannone, R. (2015). Environmental assessment of drying methods for the production of apple powders. *The International Journal of Life Cycle Assessment*, 20(12), 1659-1672.

Ergun, S. (1952). Fluid Flow Through Packed Columns. *Chemical Engineering Progress* 48, 89–94.

Fernandes, F.A.N., Linhares Jr., F.E., & Rodrigues, S. (2009). Effect of osmosis and ultrasound on pineapple cell tissue structure during dehydration. *Journal of Food Engineering*, 90, 186-190.

Floros, J.D., & Liang, H.H. (1994). Acoustically assisted diffusion through membranes. *Food Technology*, 48, 79-84.

Gallego-Juarez, J.A., Rodriguez-Corral, G., Galvez-Moraleda, J.C., & Yang, T. (1999). A new high-intensity ultrasonic technology for food dehydration. *Drying Technology*, 17, 597–608.

Gallego-Juarez, J.A., Rodriguez-Corral, G., Acosta, V.M., & Riera, E. (2010). Power ultrasonic trasducers with extensive radiators for industrial processing. *Ultrasonics Sonochemistry*, 17, 953-964.

Garcia-Pérez, J.V., Carcel, J.A., De la Fuente, S., & Riera, E. (2007). Ultrasonic drying of foodstuff in a fluidized bed: Parametric study. *Ultrasonics*, 44, 539 – 543.

Gallego-Juarez, J.A., Riera, E., De la Fuente, S., Rodriguez-Corral, G., Acosta, V.M., & Blanco, A. (2007). Application of high-power ultrasound for dehydration of vegetables: process and technology. *Drying Technology*, 25, 1893-1901.

Garcia-Perez, J.V., Ozuna, C., Ortuño, C., Cárcel, J.A., & Mulet, A. (2011). Modeling ultrasonically assisted convective drying of eggplant. *Drying Technology*, 29, 1499-1509.

Garcia-Perez, J.V., Carcel, J.A., Rossello, C., Riera, E., & Mulet, A. (2012). Intensification of low-temperature drying by using ultrasound. *Drying Technology*, 30, 1199-1208.

Garcia-Pérez, J.V., Carcel, J.A., Mulet, A., Riera, E., Gallego-Juarez, J. (2015). Power ultrasonics: Application of high-intensity ultrasounds. In J.A., Gallego-Juarez, K.F., Graff (Eds.), *Ultrasonic Drying for Food Preservation* (pp. 875-910). Elsevier, Cambridge.

Gottardo, G. (2016). Dimensionamento e Controllo di un Amplificatore ad Ultrasuoni per Dispositivi Piezoelettrici. Ms.C. Thesis, Università degli studi di Padova.

Hoang, H.M., Brown, T., Indergard, E., Leducq, D., & Alvarez, G. (2016). Life cycle assessment of salmon cold chains: comparison between chilling and superchilling technologies. *Journal of cleaner production*, 126, 363-372.

Hospido, A., Davis, J., Berlin, J., & Sonesson, U. (2010). A review of methodological issues affecting LCA of novel food products. The international Journal of Life Cycle Assessment, 15(1), 44-52.

Huijbregts, M.A.J, Steinmann, Z.J.N., Elshout, P.M.F., Stam, G., Verones, F., Vieira, M.D.M., Hollander, A., & Van Zelm, R. (2016). ReCiPe2016: A harmonized life cycle impact assessment method at midpoint and endpoint level. RIVM Report 2016-0104. Bilthoven, The Netherlands. Available at: https://www.rivm.nl/en/life-cycle-assessment-lca/downloads

Incropera, F.P., & DeWitt, D. P. (1990). *Fundamentals of Heat and Mass Transfer* (3rd ed., pp. 658–660). Wiley, New York.

ISO (UNI EN) 14040 (2006a). Environmental Management - Life Cycle Assessment - Principles and Framework, International Organization for Standardization, Geneve, Switzerland.

ISO (UNI EN) 14044 (2006b). Environmental Management - Life Cycle Assessment – Requirements and Guidelines, International Organization for Standardization, Geneve, Switzerland.

Kern, D.Q. (1950). *Process Heat Transfer*, McGraw-Hill: New York, USA.

Kumar, C., Karim, M. A., & Joardder, M. U. (2014). Intermittent drying of food products: A critical review. Journal of Food Engineering, 121, 48-57.Li, S., Stawczyk, I., & Zbcinski, I. (2007). CFD model of apple atmospheric freeze drying at low temperature. *Drying Technology*, 25, 1331-1339.

Lighthill, S.J. (1978). Acoustic streaming, *Journal of Sound and Vibration*, 61, 391-418.

Meryman, H.T. (1959). Sublimation: Freeze drying without vacuum. *Science*, 130, 628–629.

Munters (2019). https://www.munters.com/en/solutions/dehumidification/ (Accessed: 18/06/2019).

Ozuna, C., Gómez, T., Riera, E., Cárcel, J.A., & García-Pérez, J.V. (2014). Influence of material structure on air-borne ultrasonic application in drying. *Ultrasonics Sonochemistry*, 21, 1235-1243.

Prosapio, V., Norton, I., & De Marco, I. (2017). Optimization of freeze-drying using a Life Cycle Assessment approach: Strawberries' case study. Journal of Cleaner Production, 168, 1171-1179.

Puaide (2019). https://italian.alibaba.com/product-detail/efficient-dehumidifier-silica-gel-desiccant-wheel-60719424036.html?spm=a2700.7724838.2017115.19.160ae09eIVnVNa. (Accessed: 18/06/2019).

Rahman, S.M.A., & Mujumdar, A.S. (2008). A novel atmospheric freeze-drying system using a vibro-fluidized bed with adsorbent. *Drying Technology*, 26, 393–403.

Sagar, V.R., & Suresh Kumar, P. (2010). Recent advances in drying and dehydration of fruits and vegetables: a review. Journal of food science and technology, 47(1), 15-26.

Sanjuán, N., Stoessel, F., & Hellweg, S. (2014). Closing data gaps for LCA of food products: estimating the energy demand of food processing. Environmental science & technology, 48(2), 1132-1140.

Santacatalina, J.V., Fissore, D., Cárcel, J.A., Mulet, A., & Garcia-Perez, J.V. (2015). Model-based investigation into atmospheric freeze drying assisted by power ultrasound. *Journal of Food Engineering*, 151, 7-15.

Scholz, K., Eriksson, M., & Strid, I. (2015). Carbon footprint of supermarket food waste. Resources, Conservation and Recycling, 94, 56-65.

Silva, V.L., & Sanjuán, N. (2019). Opening the black box: a systematic literature review of life cycle assessment in alternative food processing technologies. *Journal of Food Engineering*, 250, 33-45.

Stawczyk, J., Li, S., Witriwa-Rojchert, D., Fabisiak, A. (2008). Kinetics of atmospheric freeze-drying of apple. *Transport in Porous Media*, 66, 159-172.

Tecno-ventil (2019). Filtri a tasche (FTS). https://www.tecnoventil.it/media/FileDocumenti/FTS-Filtri-a-tasche.pdf (Accessed: 18/06/2019).

Tefrile (2019). https://tefrile.es/aplicacion-en-productos-horticulticulas/ (Accessed: 18/06/2019).

Wolff, E., & Gibert, H. (1990). Atmospheric freeze drying, part 1: Design, experimental investigation and energy saving advantages. *Drying Technology*, 8, 385-404.

List of Tables

Figure captions

Figure 1. Sketch of the lab-scale drying unit. Circles indicates the zones contributing to the total pressure drop of the system. Different mesh type indicates the cause of the pressure drop: oblique dashed lines indicate 90-degree elbows; vertical lines, T-type connections; and dots on-off valves.

Figure 2. Sketch of the industrial atmospheric freeze-drying plant.

Figure 3. System boundaries of the gate-to-gate scheme used for the LCA.

Figure 4. Average energy consumption of the ultrasound-generating system measured in the lab-scale dryer at different US intensities and operating temperatures (○ -10°C, ■ 0°C, □ 10°C, ▲ 20°C). Dotted line shows the linear relationship calculated by Eq. 9.

Figure 5. Total energy consumptions per kilogram of water removed in the lab-scale atmospheric freeze-dryer for eggplant drying at different air velocities and ultrasonic powers.

Figure 6 Relative energy consumption of the elements of the lab-scale atmospheric freeze-dryer, namely the compressor; ultrasound-generation system (US) and the heating resistance, at different ultrasound powers. Air temperature: -10°C, air velocity: 2 ms^{-1}.

Figure 7. Influence of the type of product and ultrasound intensity applied on the total energy required for AFD. Air temperature: -10°C; Air velocity: 2 ms^{-1}.

Figure 8. Relative energy consumptions of the components of the industrial atmospheric freeze-dryer: compressor, heating system, cooling system, dehumidifier and ultrasound-generation system. Air temperature: -10°C; Air velocity: 2 ms^{-1}.

Figure 9. Relative contribution of the process units of atmospheric freeze-drying of eggplant at -10ºC and 2 ms^{-1}. CC: climate change; FP: fine particulate matter formation; FD: fossil depletion; FW-Etx: Freshwater ecotoxicity; FW-EU: freshwater eutrophication; HT: human toxicity; IR: ionizing radiation; M-Etx: marine ecotoxicity; M-Eu: marine eutrophication; MD: metal depletion; POF-E: photochemical ozone formation, ecosystems; POF-HH: photochemical ozone formation, human health; SOD: Stratospheric Ozone Depletion; TA: terrestrial acidification; T-Etx: terrestrial ecotoxicity.

Figure 10. Relative contribution of the process units of atmospheric ultrasound-assisted freeze-drying with s. Product: eggplant, air temperature: -10ºC and air velocity: 2 ms^{-1}. CC: climate change; FP: fine particulate matter formation; FD: fossil depletion; FW-Etx: Freshwater ecotoxicity; FW-EU: freshwater eutrophication; HT: human toxicity; IR: ionizing radiation; M-Etx: marine ecotoxicity; M-Eu: marine eutrophication; MD: metal depletion; POF-E: photochemical ozone formation, ecosystems; POF-HH: photochemical ozone formation, human health; SOD: Stratospheric Ozone Depletion; TA: terrestrial acidification; T-Etx: terrestrial ecotoxicity.

igure 1

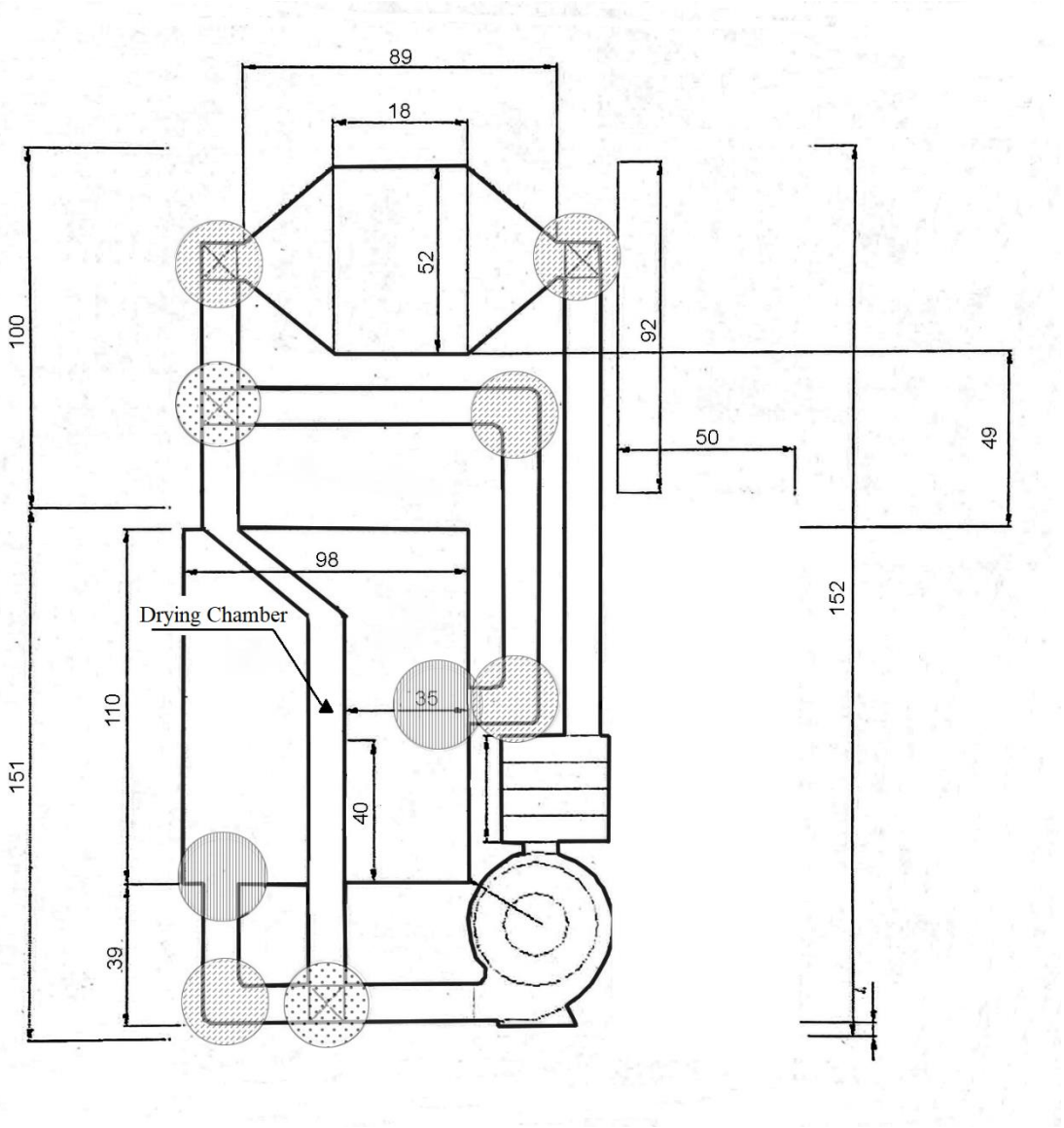

Figure 2

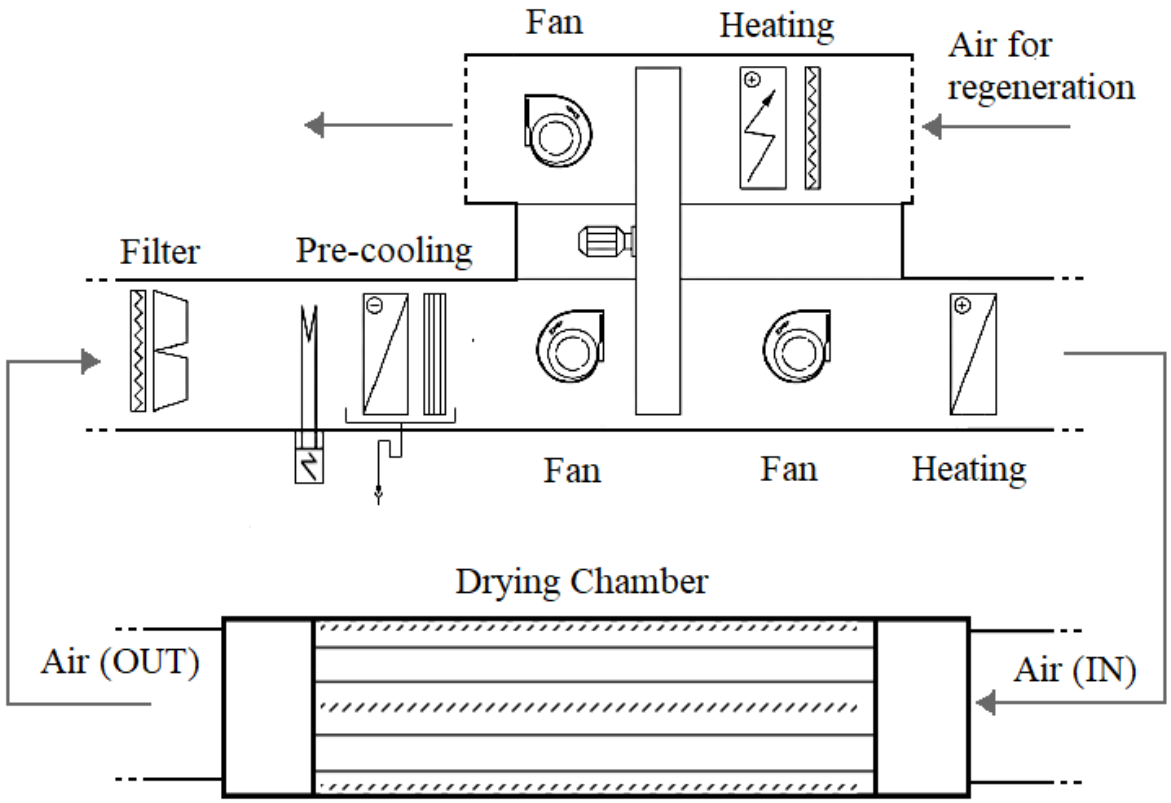
Fan
Heating
Air for regeneration
Filter
Pre-cooling
Fan
Fan
Heating
Drying Chamber
Air (OUT)
Air (IN)

Figure 3

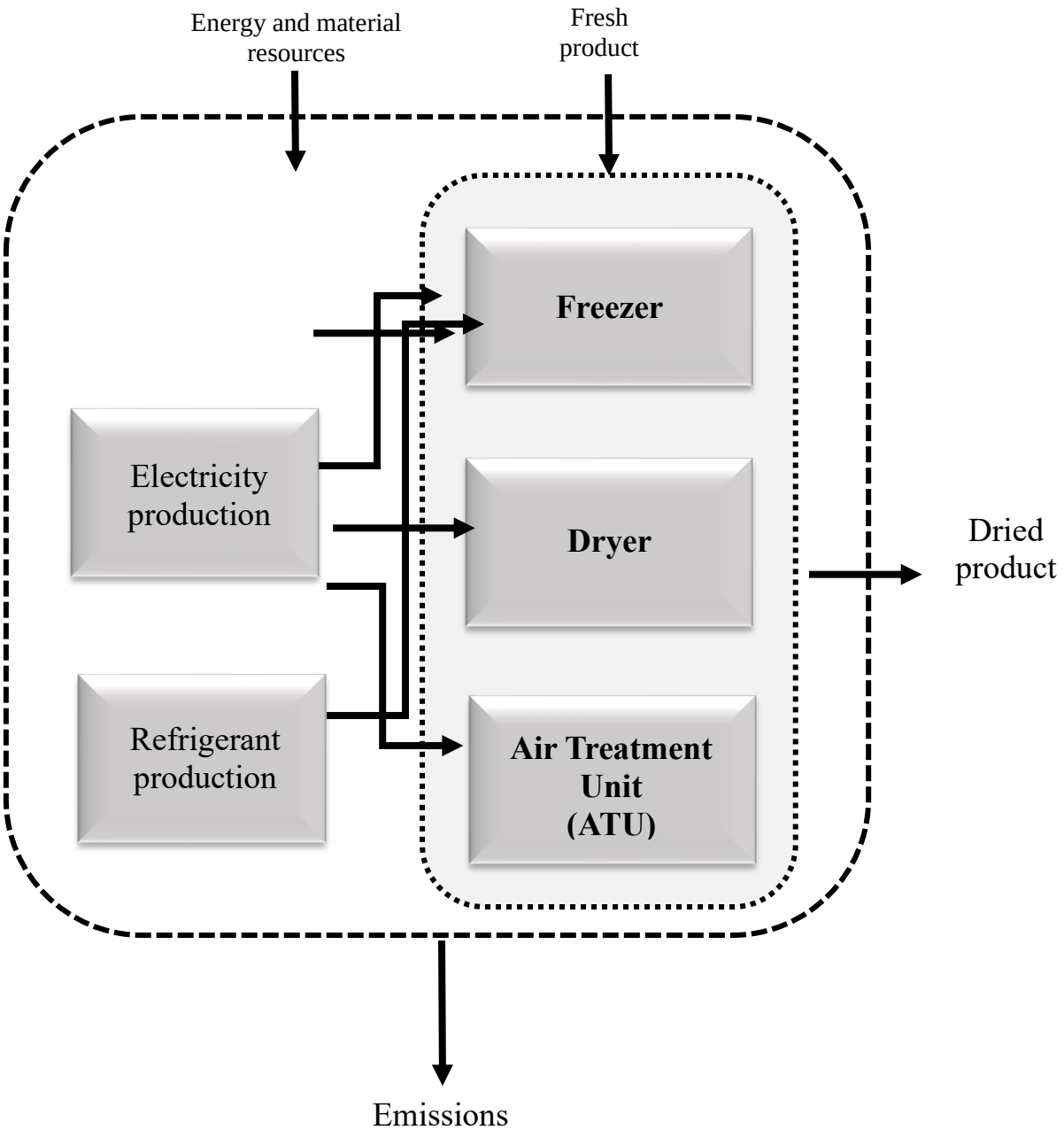
Energy and material resources
Fresh product
Freezer
Electricity production
Dryer
Dried product
Refrigerant production
Air Treatment Unit (ATU)
Emissions

Figure 4

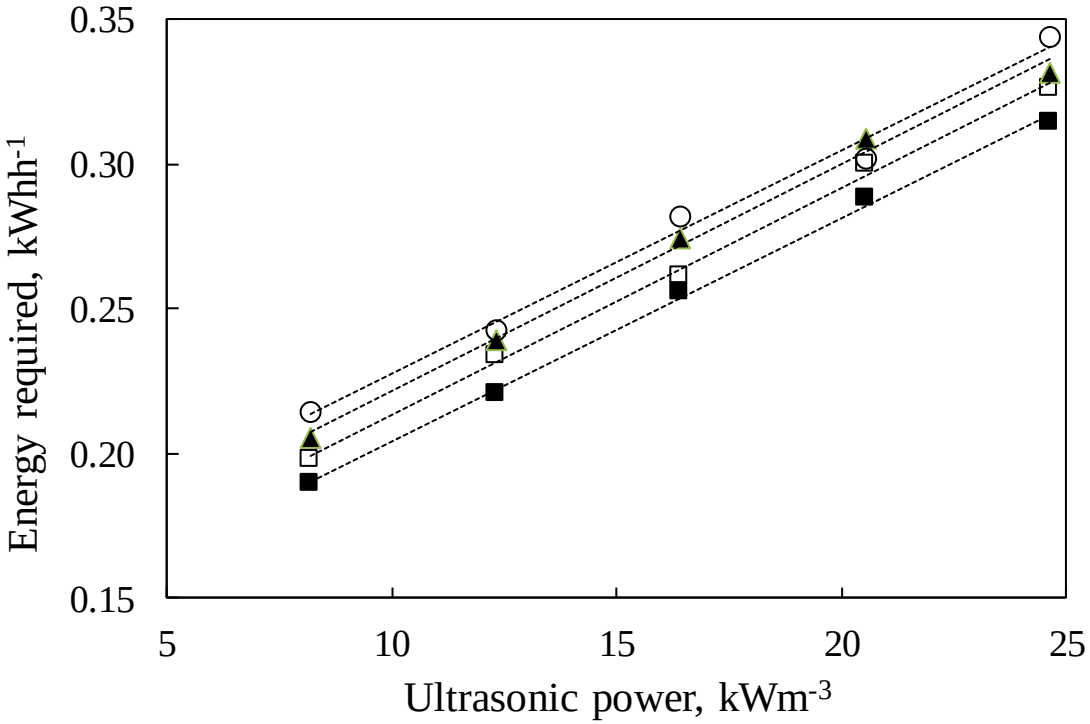
0.35
0.30
0.25
0.20
0.15
Energy required, kWhh-1
5
10
15
20
25
Ultrasonic power, kWm-3

Figure 5

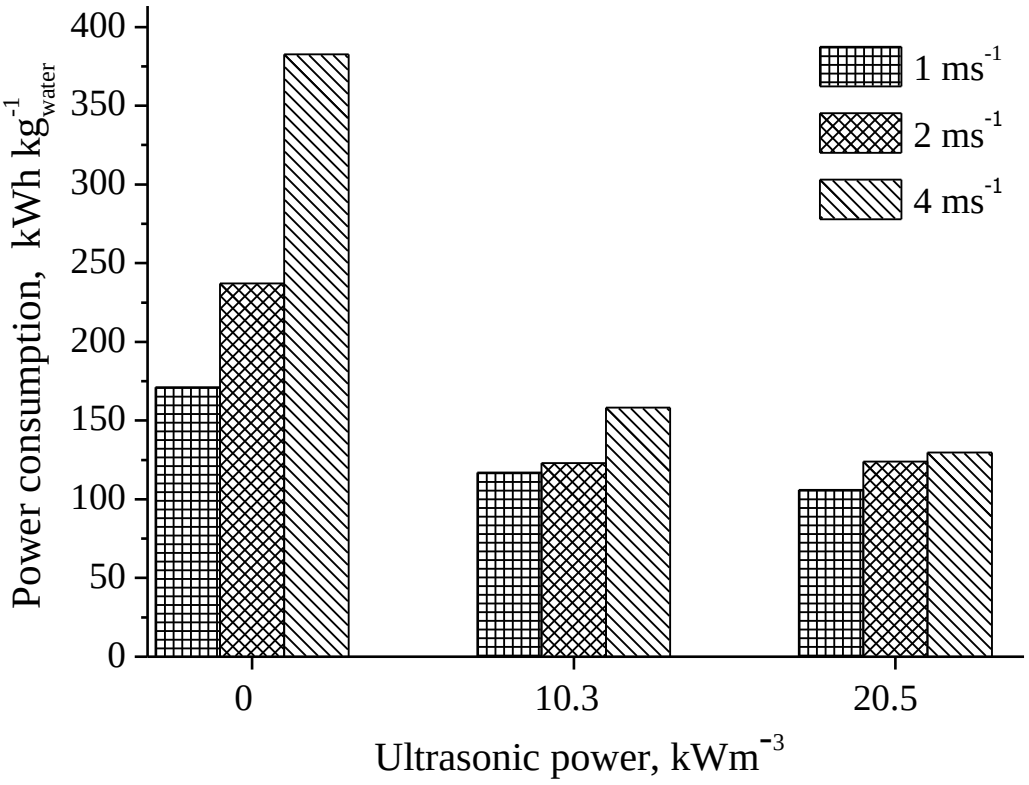
Power consumption, kWh kg$_{water}^{-1}$
400
350
300
250
200
150
100
50
0
0
10.3
20.5
Ultrasonic power, kWm^{-3}
1 ms^{-1}
2 ms^{-1}
4 ms^{-1}

Figure 6

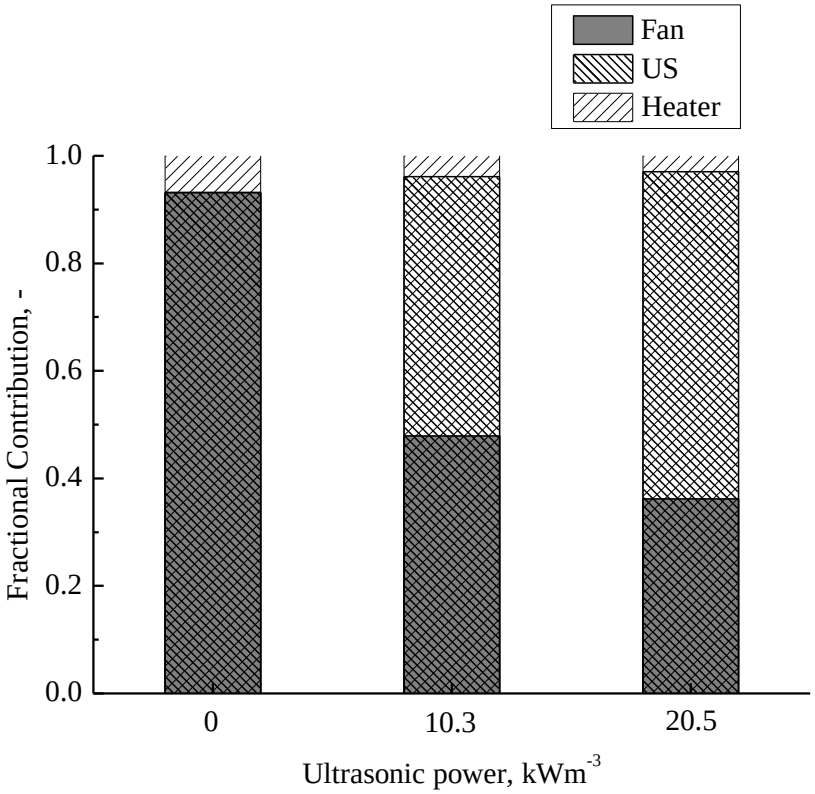
Fan
US
Heater
1.0
0.8
0.6
0.4
0.2
0.0
Fractional Contribution, -
0
10.3
20.5
Ultrasonic power, kWm-3

Figure 7

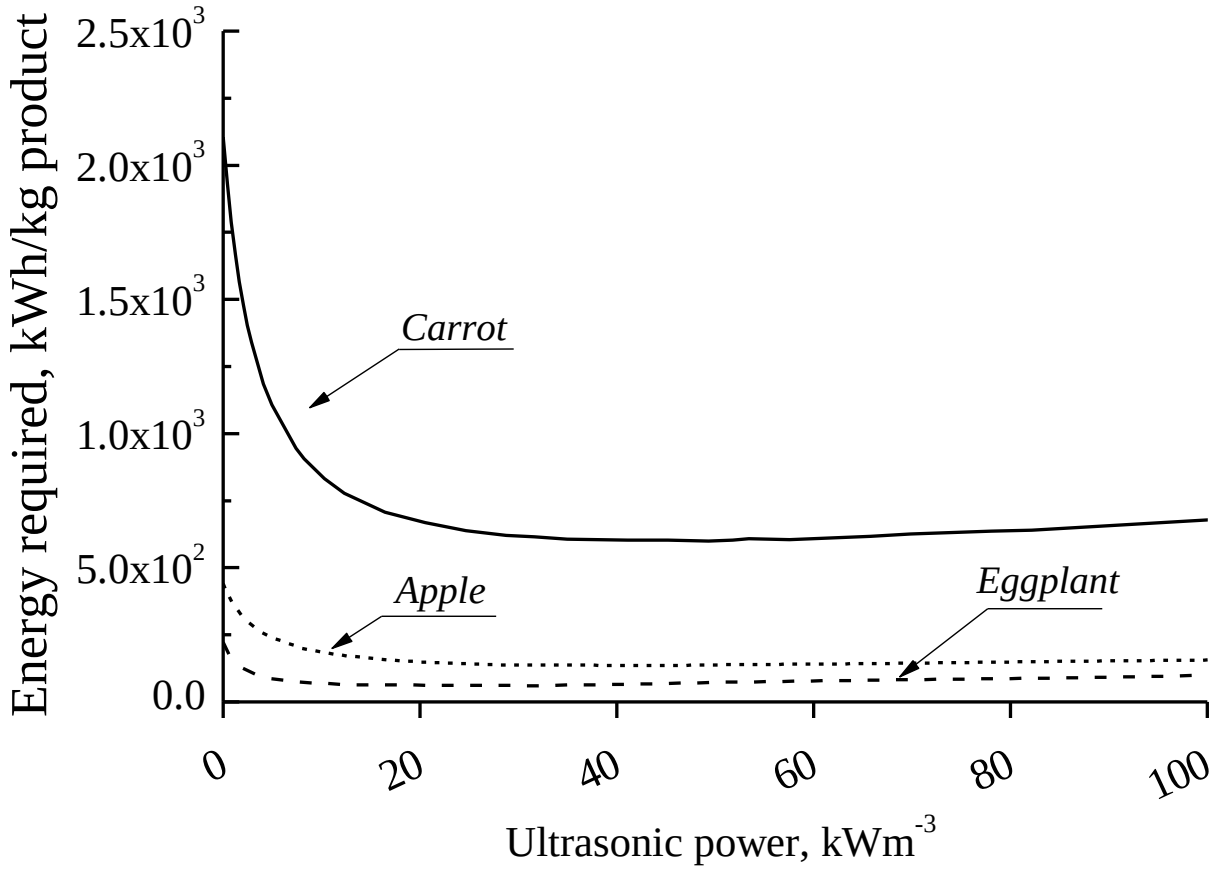
Energy required, kWh/kg product
2.5x10^3
2.0x10^3
1.5x10^3
1.0x10^3
5.0x10^2
0.0
Carrot
Apple
Eggplant
0
20
40
60
80
100
Ultrasonic power, kWm^-3

Figure 8

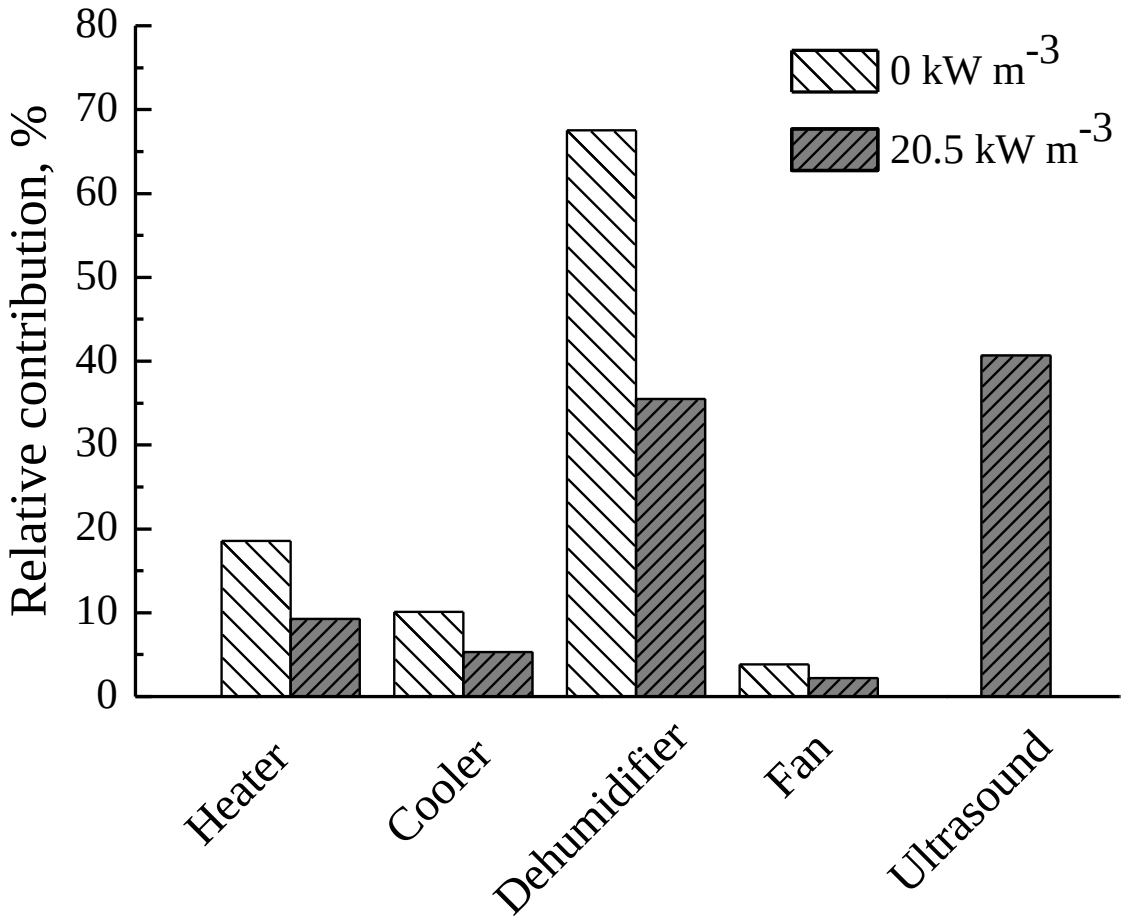
Relative contribution, %
80
70
60
50
40
30
20
10
0
0 kW m-3
20.5 kW m-3
Heater
Cooler
Dehumidifier
Fan
Ultrasound

Figure 9

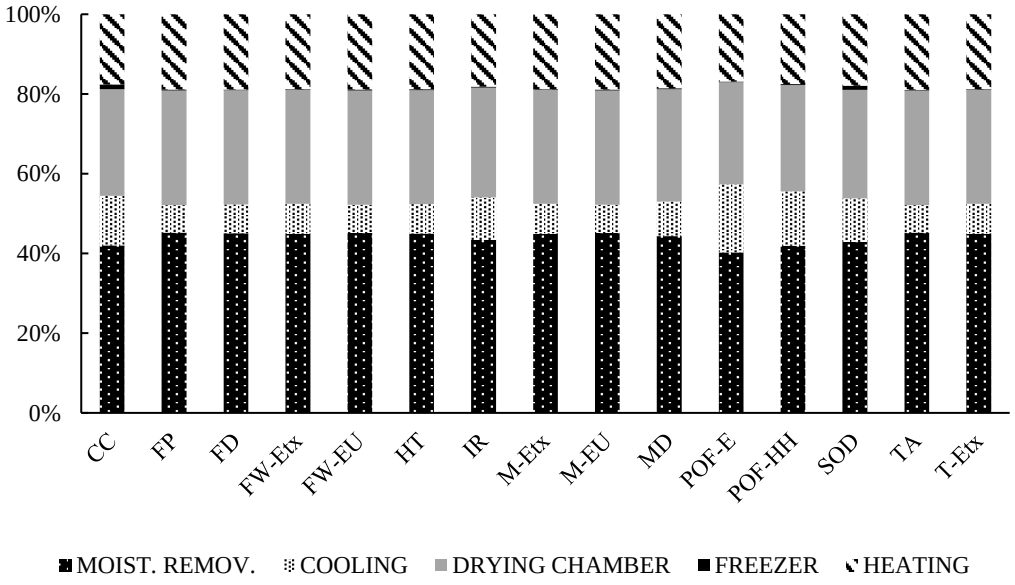
100%
80%
60%
40%
20%
0%
CC
FP
FD
FW-Etx
FW-EU
HT
IR
M-Etx
M-EU
MD
POF-E
POF-HH
SOD
TA
T-Etx
MOIST. REMOV.
COOLING
DRYING CHAMBER
FREEZER
HEATING

Figure 10

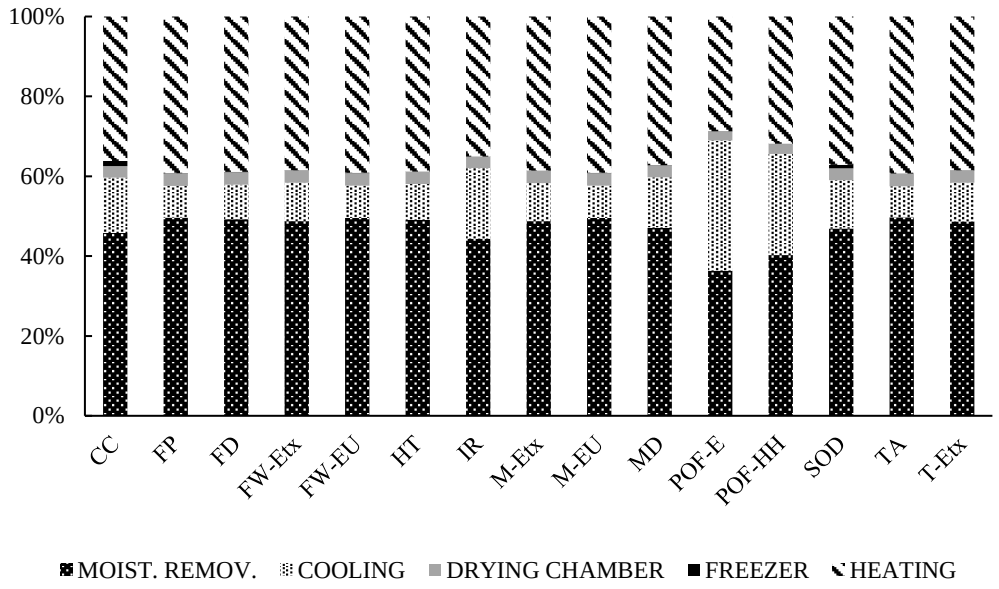
100%
80%
60%
40%
20%
0%
CC
FP
FD
FW-Etx
FW-EU
HT
IR
M-Etx
M-EU
MD
POF-E
POF-HH
SOD
TA
T-Etx
MOIST. REMOV.
COOLING
DRYING CHAMBER
FREEZER
HEATING

Table 1

Filters

FTS280-4M3 – G4		FTS280-4M3 – F7	
Number of bags	3	Number of bags	3
Surface, m^2	1	Surface, m^2	5.1
$\Delta P_{, initial}$, Pa	25	$\Delta P_{, initial}$, Pa	50
$\Delta P_{, regeneration}$, Pa	450	$\Delta P_{, regeneration}$, Pa	450

Dessicant wheel Pauide PAD-D11000K		**Cooling system**	
Air flow, $m^3 h^{-1}$	4000	Cooling power, kW	8.4
Capacity, $kg_{water} h^{-1}$	78	Nominal power, kW	11.8
Rotor velocity, rpm	10	Steady state Temperature, °C	-12/-30
Air split, %	36	Volumetric flow, $m^3 h^{-1}$	1.4
Diameter, m	1.15	Dimensions, m	1.86 x 0.74 x 1.447
Thickness, m	0.2	Technical fluid	R-404

Table 2

Parameter	Scenario
Electricity mix	Spain (ES)
	Germany (DE)
	Norway (NO)
Alternatives for impact reduction	Photovoltaic panels (Photov)
	Refrigerant R152a (152A)

Table 3

	Eggplant			Apple			Carrot		
	Ultrasound intensity		Impact reduction %	Ultrasound intensity		Impact reduction %	Ultrasound intensity		Impact reduction %
	0 (kW m^{-3})	20.5 (kW m^{-3})		0 (kW m^{-3})	20.5 (kW m^{-3})		0 (kW m^{-3})	20.5 (kW m^{-3})	
Climate change, default, excl biogenic carbon (kg CO2 eq.)	117	35.6	69.6	318	129	59.4	931	351	62.3
Fine particulate matter formation (kg PM2.5 eq.)	$1.8\cdot10^{-01}$	$6.0\cdot10^{-02}$	69.5	$5.0\cdot10^{-01}$	$2.0\cdot10^{-01}$	58.8	1.45	0.56	61.6
Fossil depletion (kg oil eq.)	35.9	10.90	69.6	99.0	40.2	59.4	301	110	63.5
Freshwater ecotoxicity (kg 1,4 DB eq.)	$4.1\cdot10^{-01}$	$1.2\cdot10^{-01}$	69.8	1.15	$4.6\cdot10^{-01}$	60.4	3.67	1.3	65.4
Freshwater Eutrophication (kg P eq.)	$2.67\cdot10^{-02}$	$8.2\cdot10^{-03}$	69.5	$7.0\cdot10^{-02}$	$3.0\cdot10^{-02}$	59.0	0.22	$8.0\cdot10^{-02}$	62.2
Human toxicity (kg 1,4-DB eq.)	51.8	15.70	69.7	144	57.9	59.7	445	160	64.0
Ionizing Radiation (Bq C-60 eq. to air)	$9.1\cdot10^{-01}$	$2.6\cdot10^{-01}$	71.5	3.0	1.01	66.4	12.9	3.21	75.1
Marine ecotoxicity (kg 1,4-DB eq.)	$5.7\cdot10^{-01}$	$1.7\cdot10^{-01}$	69.77	1.6	$6.4\cdot10^{-01}$	60.2	5.1	1.78	65.1
Marine Eutrophication (kg N eq.)	$2.1\cdot10^{-03}$	$6.39\cdot10^{-04}$	69.5	$5.7\cdot10^{-03}$	$2.3\cdot10^{-03}$	58.9	$1.67\cdot10^{-02}$	$6.4\cdot10^{-03}$	62.0
Metal depletion (kg Cu eq.)	$6.1\cdot10^{-02}$	$1.82\cdot10^{-02}$	70.5	$1.9\cdot10^{-01}$	$6.9\cdot10^{-02}$	62.9	$6.8\cdot10^{-01}$	$2.0\cdot10^{-01}$	70.2
Photochemical Ozone Formation, Ecosystems (kg NO_x eq.)	$2.8\cdot10^{-01}$	$7.0\cdot10^{-02}$	74.9	1.22	$3.1\cdot10^{-01}$	74.1	7.0	1.2	82.1
Photochemical Ozone Formation, Human Health (kg NO_x eq.)	$2.5\cdot10^{-01}$	$6.7\cdot10^{-02}$	73.3	$9.6\cdot10^{-01}$	$2.8\cdot10^{-01}$	70.8	4.9	1.0	79.7
Stratospheric Ozone Depletion (kg CFC-11 eq.)	$7.7\cdot10^{-05}$	$2.4\cdot10^{-05}$	69.5	$2.1\cdot10^{-04}$	$8.6\cdot10^{-05}$	58.8	$6.0\cdot10^{-04}$	$2.31\cdot10^{-04}$	61.2
Terrestrial Acidification (kg SO_2 eq.)	$7.8\cdot10^{-01}$	$2.4\cdot10^{-01}$	69.4	2.1	$8.7\cdot10^{-01}$	58.6	6.1	2.4	61.2
Terrestrial ecotoxicity (kg 1,4-DB eq.)	71.8	21.7	69.8	202.3	80.2	60.3	647.1	224.1	65.4

Table 4

	152A	**Photov**	**NO**	**ES**	**DE**
Climate change, default, excl biogenic carbon (kg CO2 eq.)	33.14	5.75	2.77	23.8	46.9
Fine Particulate Matter Formation (kg PM2.5 eq.)	$5.6 \cdot 10^{-02}$	$1.4 \cdot 10^{-02}$	$8.7 \cdot 10^{-04}$	$5.7 \cdot 10^{-02}$	$4.0 \cdot 10^{-02}$
Fossil depletion (kg oil eq.)	10.9	1.9	0.4	12.1	17.2
Freshwater ecotoxicity (kg 1.4 DB eq.)	$1.2 \cdot 10^{-01}$	1.3	$1.2 \cdot 10^{-02}$	$1.7 \cdot 10^{-01}$	$5.1 \cdot 10^{-01}$
Freshwater Eutrophication (kg P eq.)	$8.1 \cdot 10^{-03}$	$5.1 \cdot 10^{-03}$	$1.7 \cdot 10^{-04}$	$9.4 \cdot 10^{-03}$	$6.5 \cdot 10^{-02}$
Human toxicity (kg 1.4-DB eq.)	$1.6 \cdot 10^{+01}$	$3.0 \cdot 10^{+01}$	$8.3 \cdot 10^{-01}$	$2.0 \cdot 10^{+01}$	$7.3 \cdot 10^{+01}$
Ionizing Radiation (Bq C-60 eq. to air)	$2.5 \cdot 10^{-01}$	$4.6 \cdot 10^{-01}$	$4.6 \cdot 10^{-02}$	$1.2 \cdot 10^{+01}$	8.3
Marine ecotoxicity (kg 1.4-DB eq.)	$1.7 \cdot 10^{-01}$	1.6	$1.8 \cdot 10^{-02}$	$2.2 \cdot 10^{-01}$	$6.5 \cdot 10^{-01}$
Marine Eutrophication (kg N eq.)	$6.4 \cdot 10^{-04}$	$6.0 \cdot 10^{-04}$	$1.2 \cdot 10^{-05}$	$9.1 \cdot 10^{-04}$	$4.4 \cdot 10^{-03}$
Metal depletion (kg Cu eq.)	$1.8 \cdot 10^{-02}$	$6.6 \cdot 10^{-02}$	$7.1 \cdot 10^{-03}$	$1.8 \cdot 10^{-02}$	$1.8 \cdot 10^{-02}$
Photochemical Ozone Formation, Ecosystems (kg NO_x eq.)	$6.7 \cdot 10^{-02}$	$1.8 \cdot 10^{-02}$	$6.8 \cdot 10^{-03}$	$8.1 \cdot 10^{-02}$	$5.3 \cdot 10^{-02}$
Photochemical Ozone Formation, Human Health (kg NO_x eq.)	$6.4 \cdot 10^{-02}$	$1.7 \cdot 10^{-02}$	$4.9 \cdot 10^{-03}$	$7.9 \cdot 10^{-02}$	$5.1 \cdot 10^{-02}$
Stratospheric Ozone Depletion (kg CFC-11 eq.)	$2.2 \cdot 10^{-05}$	$2.7 \cdot 10^{-06}$	$1.3 \cdot 10^{-06}$	$8.5 \cdot 10^{-06}$	$2.8 \cdot 10^{-05}$
Terrestrial Acidification (kg SO2 eq.)	$2.4 \cdot 10^{-01}$	$2.8 \cdot 10^{-02}$	$1.9 \cdot 10^{-03}$	$1.5 \cdot 10^{-01}$	$2.1 \cdot 10^{-01}$
Terrestrial ecotoxicity (kg 1.4-DB eq.)	21.5	148.0	2.4	21.7	15.1